UNCLASSIFIED

Defense Technical Information Center
Compilation Part Notice

ADP023687

TITLE: Modeling of Surface Thermodynamics and Damage Thresholds in the IR and THz Regime

DISTRIBUTION: Approved for public release, distribution unlimited

This paper is part of the following report:

TITLE: Conference on Optical Interactions with Tissue and Cells [18th] Held in San Jose, California on January 22-24, 2007

To order the complete compilation report, use: ADA484275

The component part is provided here to allow users access to individually authored sections of proceedings, annals, symposia, etc. However, the component should be considered within the context of the overall compilation report and not as a stand-alone technical report.

The following component part numbers comprise the compilation report:
ADP023676 thru ADP023710

UNCLASSIFIED

Modeling of surface thermodynamics and damage thresholds in the IR and THz regime

C.D. Clark III[a], Robert J. Thomas[c], Paul D.S. Maseberg[b], Gavin D. Buffington[b], Lance J. Irvin[b], Jacob Stolarski[c] and Benjamin A. Rockwell[c]

[a] Northrop Grumman, 4241 Woodcock Dr. Ste B-100, San Antonio, TX, United States;
[b] Fort Hays State University, 600 Park St., Hays, KS, United States;
[c] Air Force Reasearch Lab, Human Effectivness Directorate Optical Branch, 2624 Louis Bauer Drive, San Antonio, TX, United States;

ABSTRACT

The Air Force Research Lab has developed a configurable, two-dimensional, thermal model to predict laser-tissue interactions, and to aid in predictive studies for safe exposure limits. The model employs a finite-difference, time-dependent method to solve the two-dimensional cylindrical heat equation (radial and axial) in a biological system construct. Tissues are represented as multi-layer structures, with optical and thermal properties defined for each layer, are homogeneous throughout the layer. Multiple methods for computing the source term for the heat equation have been implemented, including simple linear absorption definitions and full beam propagation through finite-difference methods.

The model predicts the occurrence of thermal damage sustained by the tissue, and can also determine damage thresholds for total optical power delivered to the tissue. Currently, the surface boundary conditions incorporate energy loss through free convection, surface radiation, and evaporative cooling. Implementing these boundary conditions is critical for correctly calculating the surface temperature of the tissue, and, therefore, damage thresholds. We present an analysis of the interplay between surface boundary conditions, ambient conditions, and blood perfusion within tissues.

Keywords: skin, laser damage, modeling, surface boundary conditions, heat transfer

1. INTRODUCTION

The theoretical understanding of laser-tissue interactions is critical to the establishment of exposure limits.[1] Our group has pursued the goal of understanding light propagation,[2,3] heat transfer, and a number of damage mechanisms[4–6] in both the eye and skin. Recently, we have focused on revisions of ANSI infrared exposure limits to more accurately reflect the trends in biological response.[7–9] This has led to a need for close examination of strongly absorbed frequencies both in the infrared (IR) and the terahertz (THz) region[10] of the electromagnetic spectrum.[7,11,12] In these regions, absorption depth of the incident radiation can be extremely shallow.[13] We have speculated that boundary conditions must be accurately represented in order to correctly predict the temperature response, and subsequent damage thresholds.

2. METHODS

We have developed a model to solve the two-dimensional, time-dependent heat equation using a finite-differencing scheme. Laser-tissue interaction is modeled using Beer's Law and linear absorption coefficients. The model is being used to predict thermal response, damage, and damage thresholds of various biological tissues exposed to laser radiation. We describe a subset of the model's capabilities, focusing on the surface boundary implementation and its effect on both temperature response and damage predictions.

Current configuration abilities allow us to model a multi-layer material of infinite radial extent. Each layer may have its own unique thermal and optical properties. Figure 1 pictures an illustration of how a sample is represented in the model. We assume azimuthal symmetry and solve the heat equation at $\theta = 0$, for $r = 0 \leftrightarrow r_{max}$ and $z = z_{min} \leftrightarrow z_{max}$. The "ghost" image on the left-hand side of Figure 1 signifies that the space is not calculated, but is found by reflecting the solution on the right-hand side across $r = 0$.

Surface boundary conditions not only effect the temperature response of the tissue, but the predicted damage for a given laser exposure. We initially intended to investigate the effect of surface boundary conditions on the damage threshold, and

Optical Interactions with Tissue and Cells XVIII, edited by Steven L. Jacques, William P. Roach,
Proc. of SPIE Vol. 6435, 643505, (2007) · 1605-7422/07/$18 · doi: 10.1117/12.700477

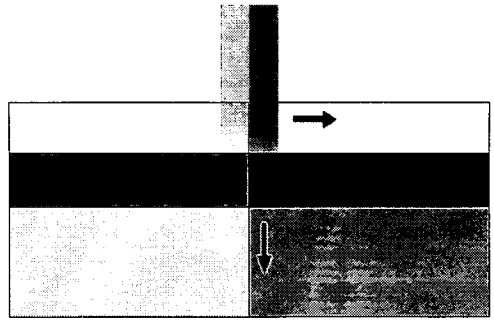

Figure 1: Illustration of how the model represents a sample and laser exposure. Only the right-hand side ($r > 0$) is actually calculated.

determine for what absorption coefficients it becomes important. However, our modeling shows a significant effect across the range of all absorption coefficients we modeled, which are typical of biological tissue.

We also discuss the importance of including perfusion when modeling damage in biological tissues with a blood flow and a surface boundary condition. It is generally accepted that perfusion is not important for calculating damage, except at long exposure durations.[14] This is true for tissues like the retina that have no surface boundary, but we will show that perfusion greatly impacts the equilibrium temperature distribution of a tissue with surface boundaries.

2.1. 2-D Cylindrical Heat Equation and Boundary Conditions

The Heat Equation is:

$$\rho c \frac{\partial T}{\partial t} = \nabla \cdot \kappa \nabla T + A$$

where T is the temperature, ρ is the density, c the specific heat, κ the conductivity, and A is a source term(s). Working in 2D cylindrical coordinates and temperature rise, rather than absolute temperature, we can express the Heat Equation as:

$$\begin{aligned} \rho(z)c(z)\frac{\partial v(z,r;t)}{\partial t} &= \frac{\kappa(z)}{r}\frac{\partial v(z,r;t)}{\partial r} + \frac{\partial}{\partial r}\left(\kappa(z)\frac{\partial v(z,r;t)}{\partial r}\right) \\ &\quad + \frac{\partial}{\partial z}\left(\kappa(z)\frac{\partial v(z,r;t)}{\partial z}\right) + A(z,r;t) \end{aligned} \tag{1}$$

where v is the temperature rise and ρ, c, and κ are assumed to be functions of z. We can also make a distinction between sources arising from external sources (laser, etc.), and those from internal sources (perfusion, etc.), so that $A(z,r;t) = A_I(z,r;t) + A_E(z,r;t)$

Currently, three separate surface boundary conditions are modeled; convection, radiation, and evaporation. They are represented by the following equations:

Convection:

$$\kappa \frac{dv}{dz} = -h_c\,(T_\infty - T) \tag{2}$$

Radiation:

$$\kappa \frac{dv}{dz} = -\sigma\epsilon\left(T_\infty^4 - T^4\right) \tag{3}$$

Evaporation:

$$\kappa \frac{dv}{dz} = -Q_{vap}\,(T, T_\infty, RH) \tag{4}$$

where h_c is the convective heat transfer rate, σ is the Steffan-Boltzmann constant, and ϵ is the emissivity of the tissue. T_∞ is the ambient temperature of the environment, and T is the tissue temperature at the surface, both in Kelvin. Q_{vap} is a heat loss function of surface temperature, ambient temperature, and ambient relative humidity due to evaporation. [15,16] A particular simulation may use these boundary conditions individually or in combination.

2.2. Numerical Solution

Equation 1 can be represented with a finite difference equation as follows:

$$\begin{aligned}\rho_i c_i \frac{v_{i,j}^{n+1} - v_{i,j}^{n}}{t^{n+1} - t^{n}} &= \frac{\kappa_i}{r_j}\left[\frac{v_{i,j+1}^{n} - v_{i,j-1}^{n}}{r_{j+1} - r_{j-1}}\right] \\ &+ \frac{2\kappa_i}{r_{j+1} - r_{j-1}}\left[\frac{v_{i,j+1}^{n} - v_{i,j}^{n}}{r_{j+1} - r_j} - \frac{v_{i,j}^{n} - v_{i,j-1}^{n}}{r_j - r_{j-1}}\right] \\ &+ \frac{2\kappa_i}{z_{i+1} - z_{i-1}}\left[\frac{v_{i+1,j}^{n} - v_{i,j}^{n}}{z_{i+1} - z_i} - \frac{v_{i,j}^{n} - v_{i-1,j}^{n}}{z_i - z_{i-1}}\right] \\ &+ \frac{\kappa_{i+1} - \kappa_{i-1}}{z_{i+1} - z_{i-1}}\left[\frac{v_{i+1,j}^{n} - v_{i-1,j}^{n}}{z_{i+1} - z_{i-1}}\right] + A_{i,j}^{n}\end{aligned} \tag{5}$$

Here the indicies i, j and n represent points in z, r and time, respectively, such that if we have spacial and temporal steps; dz, dr, dt, then

$$\begin{aligned} z_i &= i \cdot dz \\ r_j &= j \cdot dr \\ t_n &= n \cdot dt \end{aligned}$$

and

$$v_{i,j}^{n} = v(z, r; t) = v(i \cdot dz, j \cdot dr; n \cdot dt)$$

At the surface boundary, $z = 0$, the terms at $i - 1 = -1$ in Equation 5 are not known. To handle these points the boundary condition equations 2 - 4 are written in their finite difference form. Noting that the boundary condition equations are evaluated at $i = 0$, we have:

Convection:

$$\kappa \frac{v_{1,j} - v_{-1,j}}{z_1 - z_{-1}} = -h_c\,(T_\infty - T_0) \tag{6}$$

Radiation:

$$\kappa \frac{v_{1,j} - v_{-1,j}}{z_1 - z_{-1}} = -\sigma\epsilon\left(T_\infty^4 - T_0^4\right) \approx -\sigma\epsilon T_\infty^3\,(T_\infty - T_0) \tag{7}$$

Evaporation:

$$\kappa \frac{v_{1,j} - v_{-1,j}}{z_1 - z_{-1}} = -Q_{vap}\,(T_0, T_\infty, RH) \tag{8}$$

The radiative boundary condition in Equation 7 is linearized by the approximation $\left(T_\infty^4 - T_0^4\right) \approx 4T_\infty^3\,(T_\infty - T_0)$. These equations can be used to solve for the unknown points at $i - 1 = -1$ and substituted into Equation 5.

3. RESULTS/DISCUSSION

3.1. Equilibrium and Initial Conditions

We should clarify a few of the terms we will be using in our descriptions. When talking about surface boundary conditions, we mention ambient conditions. These are the conditions of the environment, specifically the temperature and relative humidity of the air outside the tissue. Initial conditions refer to the initial temperature distribution within the modeled tissue when a simulation begins. The equilibrium temperature distribution, or equilibrium state, is the time-independent temperature distribution throughout the tissue that is reached if the model is run out to long times *. The equilibrium temperature distribution depends on both the boundary conditions, and the source term. When we talk about the equilibrium state, we are referring to the case with no external source term ($A_E = 0$).

*Typically hunderds of seconds

We have the ability to load an initial temperature distribution into the model before a simulation begins. By default, the initial temperature distribution is one uniform temperature across the entire tissue. Typically, the front boundary is configured to be a surface, while the back side acts as a sink ($\Delta T = 0$), so that the tissue temperature is held to the initial baseline temperature at the back boundary, but is allowed to cool at the front surface boundary. We can run a simulation without laser exposure for a sufficiently long time, until the tissue cools to it's equilibrium state, and load this temperature distribution as an initial condition for subsequent simulations.

Laser exposures are simulated by calculating the source term A_E generated by the laser, and inserting it into Equation 5. With the typical configuration described above, heat reaching the back boundary is removed from the system. Generally this is not desired, so the back boundary is set far enough away from the front surface that heat will not reach it within the simulation time.

3.1.1. Surface Temperature and Axial Temperature Gradient

If the system is not in a semi-equilibrium state before the laser exposure is simulated, the heat generated by the laser can be less than the heat lost at the surface boundary. With a negative net heat at the surface, no surface temperature rise will be calculated. Initial conditions therefore play an important part in correctly predicting the surface temperature rise.

The body has a core temperature of 37° C, while the surface temperature of the skin has been reported to be between 28°and 35°.[17] If the tissue temperature is initially set to 37°, then the surface temperature should cool to somewhere between 28°- 35°, and there will be a temperature gradient through the tissue.

The one-dimensional case gives an idea of what this temperature gradient looks like. If the r boundary is sufficiently far away, the axial temperature distribution at $r = 0$ can be treated as a one-dimensional problem. Now, if there is no blood flow, or other source of internal heat generation, the equilibrium temperature distribution is described by the Laplacian:

$$\nabla^2 v = 0$$

where we are only looking at a single, homogeneous tissue. In one dimension, this becomes:

$$\frac{d^2 v}{dz^2} = 0 \tag{9}$$

The solution to Equation 9 is a straight line. However, if the tissue has a blood flow through it, the effect of the blood can be approximated by a source term of the following form:[14]

$$A_I(z, r; t) = \gamma c v$$

where γ is the blood flow rate and c the specific heat of the blood. Equation 9 is modified to the following form:

$$\kappa \frac{d^2 v}{dz^2} + \gamma c v = 0 \tag{10}$$

and the solution is:

$$v(z, r; t) = A\left(e^{\beta z} + e^{-\beta z}\right) \tag{11}$$

where A and β are constants determined by the boundary conditions.

Looking at a purely convective surface boundary (Equation 2) on the front surface, with the back surface set to a sink, a typical axial temperature distribution is shown in Figure 2 † for a baseline tissue temperature of 37° C and an ambient temperature of 20° C, where the surface boundary condition is at $z = 0$, and a sink is at $z = 2$. Solutions to both Equation 9 and Equation 10 are shown. As expected, the surface of a non-perfused tissue will cool to a lower temperature than that of a perfused tissue. The equilibrium surface temperature depends on the ambient conditions, but we would expect the thickness of the tissue to also affect the surface temperature, since the back boundary is essentially an infinite heat bath from which energy can enter or leave the system as needed.

†Here we have used a convective heat transfer rate, h_c representative of a "wet" surface, effectively simulating cooling due to evaporation. When the evaporative boundary condition is modeled, an h_c term corresponding to a "dry" surface is used.

3.1.2. Effect of Tissue Thickness

Figure 3 shows the surface temperature as a function of tissue thickness for both Equations 9 and 10. Equilibrium surface temperature decreases as the back boundary, held to a constant temperature, is moved away. The surface temperature approaches a limit which is the minimum temperature the surface would cool to if the tissue were infinitely thick. For the non-perfused tissue described by Equation 9, this limit is just the ambient temperature. For a perfused tissue, the limit depends on the thermal properties of the tissue, blood, and the specific boundary conditions.

We define the "critical thickness" to be the tissue thickness at which the equilibrium surface temperature is within 1% of the surface temperature of an infinitly thick tissue. With this definition, the critical thickness of the two cases shown in Figure 3 are 1.35 cm and 132 cm for the perfused and non-perfused cases respectively. The non-perfused critical thickness is much larger than the scale we are interested in modeling.

Even though the surface temperature becomes constant past the critical thickness, the axial temperature distribution within the tissue cannot be the same. Figure 4 shows the axial temperature distribution at equilibrium for tissue thicknesses of 2 and 6 cm. The thickness are much smaller than the non-perfused critical thickness, so the equilibrium states are drastically different. The 6-cm tissue's temperature is 13% lower than the 2-cm tissue at the surface and 25% lower at 2-cm tissue thickness. However, the two perfused tissue temperature profiles look essentially the same, and in fact the difference in temperature between the 2-cm and 6-cm perfused tissues is never more than 0.5%.

Figure 4 illustrates the importance of perfusion when modeling surface boundaries. In non-perfused tissues, the equilibrium state is significantly affected by the tissue thickness. It is not sufficient to configure the model to some arbitrary thickness, because this will ultimately impact the final results. However, for perfused tissues, the equilibrium state is virtually unaffected past the critical thickness for the given boundary conditions. This is especially true if we are modeling highly absorbed wavelengths (See Section 3.2.1), where most of the energy is being absorbed within the first millimeter or so. The equilibrium state is effectively the same for the 2 cm and 6 cm tissues over the penetration depth of the wavelength.

If the actual thickness of a perfused tissue being modeled is greater than the critical thickness, then any model size larger than the critical thickness will suffice in representing the tissue. Or, perhaps more useful, a thick tissue with blood flow can be sufficiently represented by it's critical thickness[‡].

3.1.3. Effect of Ambient Conditions

The equilibrium state of the system depends on the surface boundary conditions, which in turn depend on the ambient temperature through convection and evaporation; the relative humidity through evaporation; and the emissivity of the tissue through radiation. Of these three, relative humidity and ambient temperature have the largest effect. Figure 5 shows how the equilibrium surface temperature is affected by the ambient temperature at various humidities. Typically, the environment is modeled to be 20°C with 50% relative humidity, which gives a surface temperature around 32.3°C. This compares to the literature.[17]

3.2. Damage Threshold Predictions

Tissue damage is modeled by the Arrhenius damage integral:

$$\Omega(z, r; \tau) = A \int_0^{\tau} exp\left(\frac{-E_a}{RT(z, r; t)}\right) dt \tag{12}$$

where R is the universal gas constant and T is the temperature measured in Kelvin. A is a normalization constant and E_a is the action potential specific to the tissue. Values for A and E_a can be found in the literature.[14] For modeled tissue representative of skin, we used $A = 3.1 \times 10^{98}$ and $E_a = 6.28 \times 10^5$. Damage is usually defined as $\Omega = 1$, which corresponds to irreversible thermal damage.[14] These parameters give results that compare well with previous modeling efforts, and experimental validation.[11]

[‡]As mentioned earlier in this section, this is not true if heat will reach the back boundary within the simulation time.

3.2.1. Linear Absorption and Thermal Response

The source term $A_E(z, r; t)$ in Equation 1 is calculated using Beer's Law:

$$A_E(z, r; t) = I_0(r; t)\mu_a(z, \lambda)\ e^{-\mu_a(z,\lambda)\, z} \tag{13}$$

where μ_a is the linear absorption coefficient, specific to a tissue and wavelength, and I_0 is the incident irradiance distribution[§].

Surface boundary conditions impact the tissue's thermal response in two ways. First, they control the rate at which heat is allowed to leave the tissue at the surface, and will change the surface temperature rise for a given exposure. Secondly, they affect the equilibrium surface temperature. Figure 6 shows the maximum surface temperature rise of four simulations. Two cases were run with the default initial conditions, constant uniform tissue temperature. One was run with low ambient temperature and relative humidity, 10°C and 10%, the other with high ambient temperature and relative humidity, 30°and 90%.

The other two cases in Figure 6 were run under the same ambient conditions as the two cases described above, but with an equilibrium initial condition.

3.2.2. Effect of Initial/Ambient Conditions on Damage Predictions

Figure 7 shows predicted damage thresholds as a function of absorption coefficient for a typical boundary condition configuration at three different exposure durations, 1 μs, 0.1 s and 10 s. Core temperature was assumed to be 37 °C, with an ambient temperature of 20 °C and 50% relative humidity. Initial conditions were the equilibrium state. For a given exposure duration, damage threshold's generally decrease as the absorption coefficient increases. But, as shown in Figure 7, for a given exposure duration, there is a point where increasing the absorption coefficient no longer decreases the damage threshold. This point occurs at lower absorption coefficients for longer exposure durations.

Figure 8 is a comparison of the 10-second exposure predicted damage threshold for a perfused and non-perfused configuration with equilibrium initial conditions, as well as a perfused configuration with the default initial conditions (uniform temperature). All cases use the same ambient conditions (those used in Figure 7), but have completely different initial conditions as discussed in Section 3.1. Damage thresholds are about 25% higher in the non-perfused tissue than the perfused tissue, under the same ambient conditions. On the other hand, modeling a perfused tissue, but not loading the equilibrium initial conditions gave damage predictions that were 13% lower.

Assuming that the modeled tissue does have a blood flow, damage predictions can still be affected by different ambient conditions, although the effect should not be as large as the difference observed in the perfused/non-perfused cases. We ran simulations over a range of ambient conditions, and the two sets of conditions that gave the largest deviation from the conditions modeled in Figures 7 and 8 were 10 °C ambient temperature with 10% humidity and 30 °C with 90% humidity. Figure 9 pictures the typical ambient condition configuration along with the two extreme cases described. The 'warmer' climate (30 °C, 90% RH) lowers the damage threshold by ~10%, while the 'colder' climate raises the threshold ~7%'.

4. CONCLUSIONS

The work presented here demonstrates the interplay between surface boundary conditions, ambient conditions, tissue properties, and initial condition assumptions in the modeling of thermal damage to tissues from infrared or THz exposures. Care must be given to the selection of computational space dimensions such that the effects of perfusion are properly accounted for in both heating from surface heating exposures, and in the construction of a physically correct initial state of temperature distribution. In addition, the effect or role of each of these is demonstrated to vary as a function of exposure time.

General conclusions which can be drawn from this work are important to the analysis of modeling of damage thresholds for the purpose of establishing exposure limits. First, surface ambient and surface boundary conditions create minimal variations in predicted thermal response as a function of absorption depth in the tissues. This means that little variation in damage threshold can be anticipated with variations of exposure wavelength, or with variation of the ambient conditions during the exposure. A maximum variation of approximately 30 percent is seen in this preliminary analysis.

[§]Scattering is not currently considered in the model

Accurate representation of perfusion within the tissue is important beyond the commonly accepted assumption that it is only important for exposure durations of greater than about 10 seconds. In fact, the perfusion effects in the establishment of initial steady-state temperature distributions within the tissue is important even for short pulse durations. Perfusion rate and distribution affects the axial temperature distribution to which the tissue propagates during a time-dependent simulation, and determines the volume of tissue which must be heated in order to overcome the near-surface ambient cooling. A variation of nearly a factor of two was seen across the absorption coefficient range examined, depending upon the assumptions regarding initial and ambient conditions in the model.

Finally, a secondary outcome of this work is the discovery that the variation in absorption coefficient will affect trends in damage thresholds as a function of exposure time. Our modeling predicts the transition from a regime in which a standard action spectrum model to one which requires a more detailed thermal analysis. For example, a 10-second exposure can only be represented by a standard action spectrum for absorption coefficients up to about 10 cm^{-1}, while shorter exposures, shown in Figure 7, can extend the accuracy of the action spectrum analysis to about 100 cm^{-1}. This trend continues until the condition of Mixon-Roach is met for times much less than the thermal diffusion time. At high absorption coefficients, thermal diffusion begins to cause effects even at relatively short times. This happens because all of the energy is absorbed in a small volume, very close to the surface, and a steep temperature gradient is generated. Heat flows into the tissue, and the rate at which it flows is determined by the temperature gradient in the tissue. When the absorption coefficient decreases, the temperature gradient generated in the tissue becomes smaller as the energy is deposited over a larger volume. With a smaller temperature gradient, heat travels into the tissue slower, and it takes longer for the effect of diffusion to set in.

Acknowledgments

This work was sponsored by the United States Air Force Research Laboratory, and USAF Contract Number F4162402-D-7003. The authors would like to acknowledge support from the United States Air Force Office of Scientific Research, grant number 92HE04COR. P.D.S. Maseberg wishes to acknowledge the support of the USAF Research Laboratory Human Effectiveness Directorate Consortium Fellows Program. Opinions expressed here are those of the authors and do not constitute those of the USAF or the Department of Defense.

REFERENCES

1. B. A. Rockwell, C. P. Cain, W. P. Roach, and R. J. Thomas, "Safe use of ultrashort lasers," *Commercial and Biomedical Applications of Ultrafast Lasers* **3616**(1), pp. 32–39, SPIE, 1999.
2. C. P. Cain, R. J. Thomas, G. D. Noojin, D. J. Stolarski, P. K. Kennedy, G. D. Buffington, and B. A. Rockwell, "Sub-50-fs laser retinal damage thresholds in primate eyes with group velocity dispersion, self-focusing and low-density plasmas," *Graefe's archive for Clinical and Experimental Ophthalmology* **243**(2), pp. 101–112, 2005.
3. R. L. Vincelette, R. J. Thomas, B. A. Rockwell, and A. J. Welch, "A comparison of a first-order thermal lensing model to a closed aperature z-scan for th epropagation of light in ocular media," *Optical Interactions with Tissue and Cells XVII* **6084**(1), SPIE, 2006.
4. B. A. Rockwell, C. A. Toth, W. P. Roach, D. J. Payne, J. Richard A. Hopkins, P. K. Kennedy, D. J. Stolarski, G. D. Noojin, R. J. Thomas, and C. P. Cain, "Retinal damage mechanisms and safety for ultrashort laser exposure," *Laser-Tissue Interaction X: Photochemical, Photothermal, and Photomechanical* **3601**(1), pp. 4–10, SPIE, 1999.
5. C. P. Cain, C. D. DiCarlo, P. K. Kennedy, G. D. Noojin, R. E. Amnotte, and W. P. Roach, "In vivo laser-induced breakdown in the rabbit eye," *Laser-Tissue Interaction VI* **2391**(1), pp. 41–47, SPIE, 1995.
6. C. A. Toth, D. G. Narayan, C. Osborne, B. A. Rockwell, C. D. Stein, R. E. Amnotte, C. D. DiCarlo, W. P. Roach, G. D. Noojin, and C. P. Cain, "Histopathology of ultrashort-laser-pulse retinal damage," *Laser-Tissue Interaction VII* **2681**(1), pp. 375–381, SPIE, 1996.
7. C. P. Cain, K. J. Schuster, J. J. Zohner, K. L. Stockton, D. J. Stolarski, R. J. Thomas, B. A. Rockwell, and W. P. Roach, "Visible lesion thresholds with pulse duration, spot size dependency, and model predictions for 1.54-mu m, near-infrared laser pulses penetrating porcine skin," *Journal of Biomedical Optics* **11**(2), p. 024001, 2006.
8. G. D. Polhamus, J. A. Zuclich, C. P. Cain, R. J. Thomas, and M. Foltz, "Model predictions of ocular injury from 1315-nm laser light," *Laser and Noncoherent Light Ocular Effects: Epidemiology, Prevention, and Treatment III* **4953**(1), pp. 91–100, SPIE, 2003.
9. J. Zuclich, D. Lund, and B. Stuck, "Wavelength dependence of ocular damage thresholds in the near-ir to far-ir transition region: Proposed revisions to mpes," *Health Physics* **92**(1), pp. 15–23, 2007.

10. R. J. Thomas, J. Payne, C. D. Clark III, D. N. Goddard, J. McQuade, G. D. Buffington, P. D. S. Maseberg, S. M. Bonham, K. Yaws, M. Haeuser, and W. P. Roach, "Terahertz frequency bioeffects models," *In Preparation* , 2006.
11. B. Chen, D. C. O'Dell, S. Thomsen, B. A. Rockwell, and A. J. Welch, "Porcine skin ed50 damage thresholds for 2,000 nm laser irradiation," *Lasers in Surgery and Medicine* **37**, pp. 373–381, 2005.
12. B. Chen, R. Thomsen, Thomas, and A. J. Welch, "Modeling thermal damage in skin during 2000 nm laser irradiation," *In Preparation* , 2006.
13. A. N. Takata, D. Zaneveld, and M. S. Richter, "Sam-tr-77-38 laser induced thermal damage of skin," USAF Technical Report SAM-TR-77-38, USAF School of Aerospace Medicine, 1977.
14. A. J. Welch and M. J. C. van Gemert, *Optical-Thermal Response of Laser-Irradiated Tissue*, Lasers, Photonics, and Electro-Optics, Plenum Press, New York, first ed., 1995.
15. J. H. Torres, M. Motamedi, J. A. Pearce, and A. J. Welch, "Experimental evaluation of mathematical models for predicting the thermal response of tissue to laser irradiation," *Applied Optics* **32**(4), pp. 597–606, 1993.
16. F. P. Incropera and D. P. DeWitt, *Fundamentals of Heat and Mass Transfer*, John wiley & Sons, Inc., New York, fourth ed., 1996.
17. J. Griffith, A. Hamilton, G. Long, A. Mujezinovic, D. Warren, and K. Vij, "Human skin temperature response to absorbed thermal power," *Medical Imaging 1997: Ultrasonic Transducer Engineering* **3037**(1), pp. 129–134, SPIE, 1997.

Table 1: Symbols used through out the paper.

T	Temperature $[K]$
T_∞	Ambient (Air) Temperature $[K]$
ν	Relative Temperature Rise $[K]$
A	Source Term $\left[\frac{W}{cm^3}\right]$
I_0	Irradiance $[W]$
ρ	Density $\left[\frac{g}{cm^3}\right]$
γ	Blood Flow Rate $\left[\frac{g}{cm^3 s}\right]$
c	Specific Heat $\left[\frac{J}{g\,^\circ C}\right]$
κ	Conductivity $\left[\frac{J}{s\,cm\,^\circ C}\right]$
h_c	Convective Heat Loss Rate $\left[\frac{J}{s\,cm^2\,^\circ C}\right]$
ϵ	Emissivity
σ	Steffan-Boltzmann Constant $\left[\frac{J}{K}\right]$
Q_{vap}	Evaporative Boundary Heat Loss Function $\left[\frac{J}{s\,cm^2\,^\circ C}\right]$
μ_a	Linear Absorption Coefficients $\left[\frac{1}{cm}\right]$
λ	Wavelength $[m]$
Ω	Damage Integral
R	Universal Gas Constant $\left[\frac{J}{Mole\,K}\right]$
A	Damage Normalization Constant $\left[\frac{J}{Mole}\right]$
E_a	Damage activation energy $\left[\frac{1}{s}\right]$

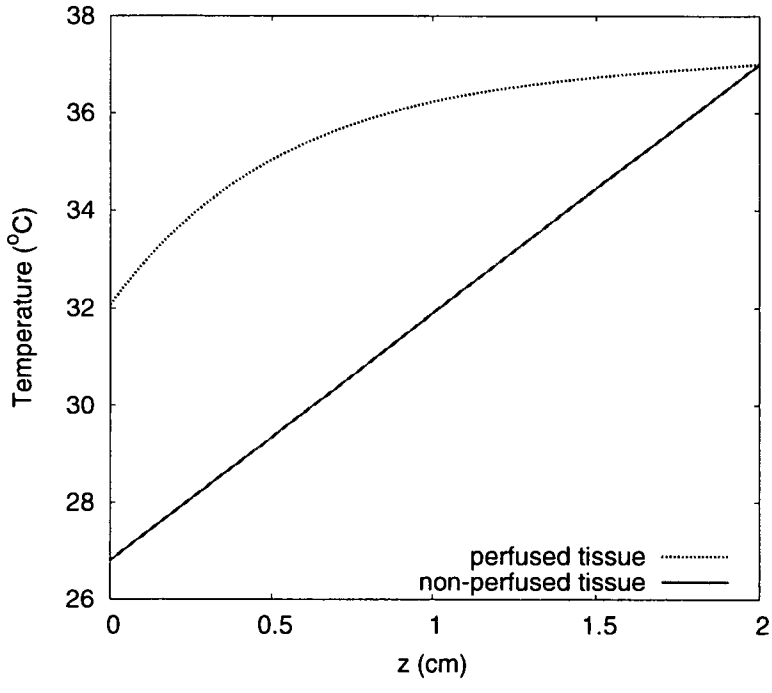

Figure 2: Axial equilibrium temperature distribution in a perfused, and non-perfused tissue.

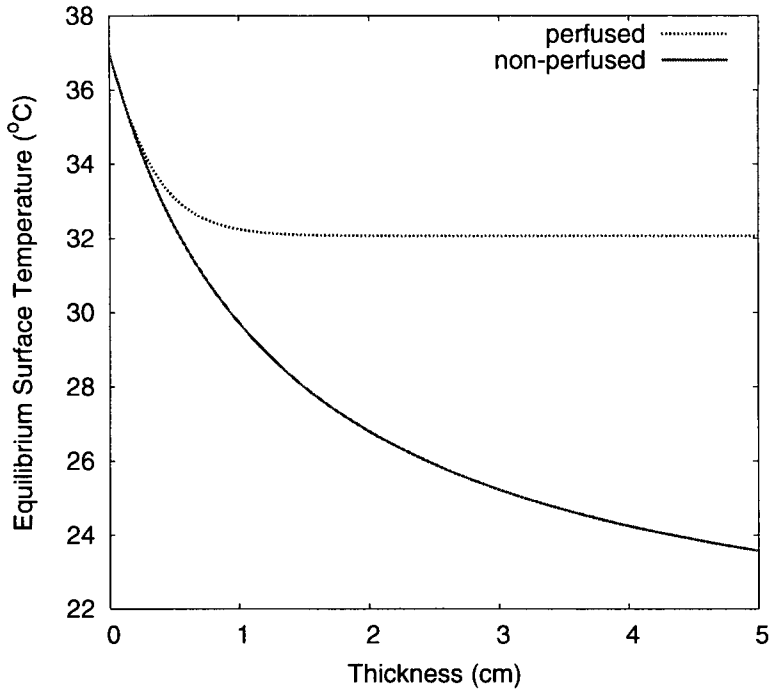

Figure 3: Equilibrium surface temperature as a function of tissue thickness for a tissue with a surface boundary at the front, ambient temperature of 20 °C, and the back boundary held to 37 °C. Temperature goes down as the sink boundary condition is moved back.

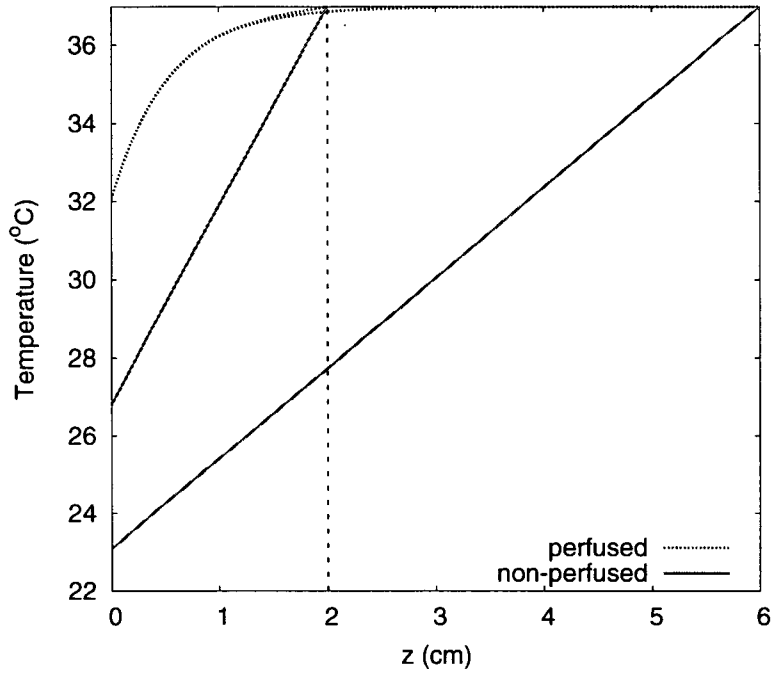

Figure 4: Equilibrium temperature distribution in perfused and non-perfused tissues of various thicknesses. Although difficult to see, there are two perfused cases shown.

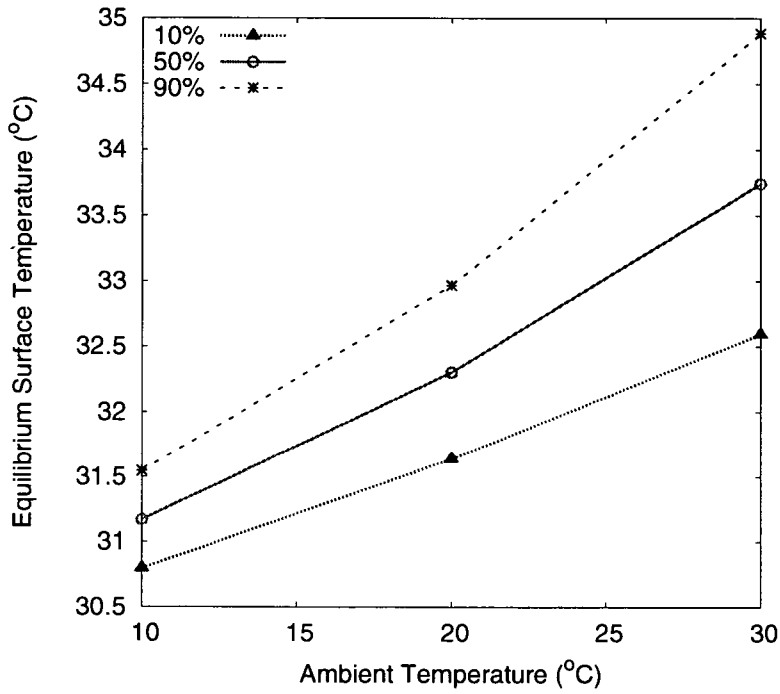

Figure 5: Equilibrium surface temperature as a function of ambient temperature at various relative humidities for a perfused tissue with a front boundary surface and the back boundary held to 37 °C.

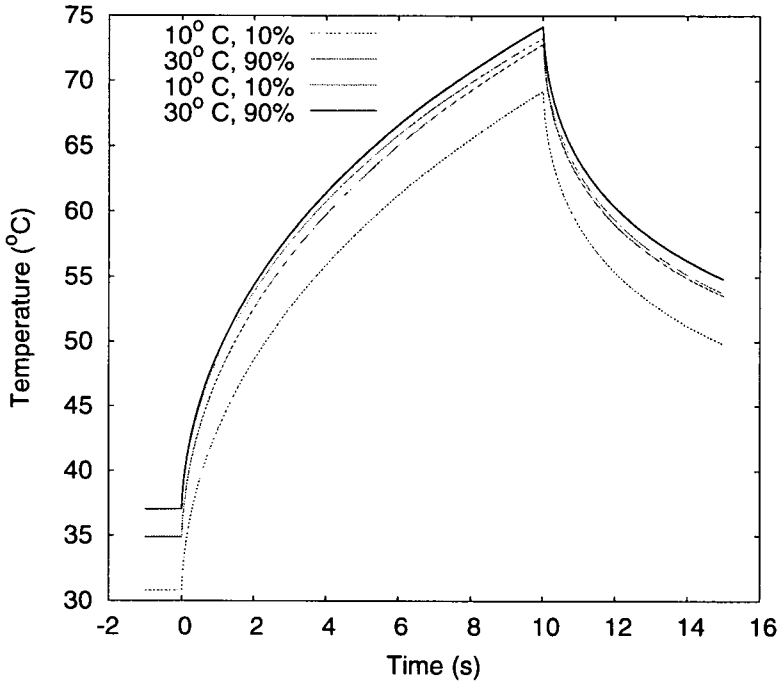

Figure 6: Surface temperature response to $2W/cm^2$ exposure for various boundary conditions and ambient temperatures. The tissue was modeled with a blood flow, a surface boundary at the front, and the back boundary held to 37 °C.

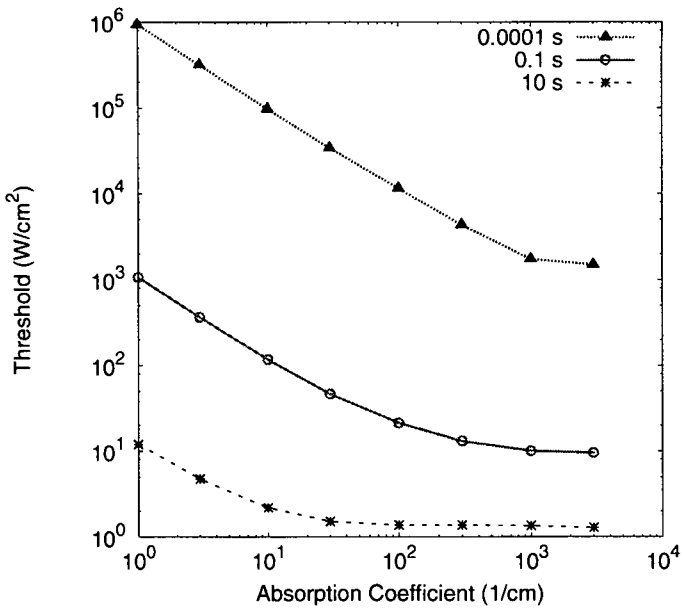

Figure 7: Damage Threshold predictions as a function of absorption coefficient. Tissue core temperature is assumed to be 37°C with an ambient air temperature of 20°C and 50% relative humidity.

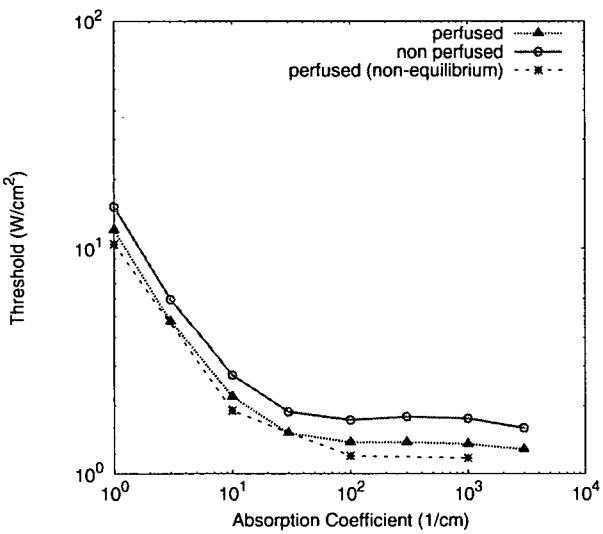

Figure 8: Effect of initial conditions for perfused and non-perfused tissues on damage threshold predictions for a 10 second exposure. Ambient conditioned were modeled as 20 °C and 50% humidity, and core temperature of 37 °C.

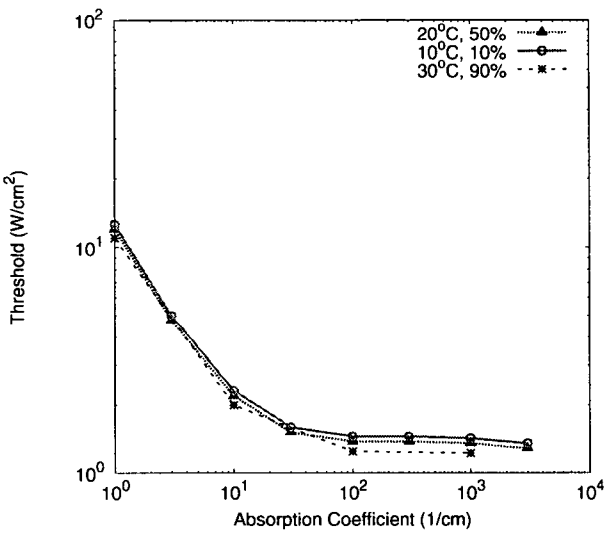

Figure 9: Effect of ambient conditions on damage threshold predictions for 10 second exposure. Ambient conditions were 20 °C and 50% humidity with 37 °C core temperature.